



Signatures of nonlocal electrical conductivity in near-field microscopy

Mikhail Khavronin and Dmitry Svintsov 

*Laboratory of 2d Materials for Optoelectronics, Center for Photonics and 2d Materials,
Moscow Institute of Physics and Technology, Dolgoprudny 141700, Russia*

 (Received 28 July 2022; revised 13 April 2023; accepted 10 May 2023; published 19 May 2023)

We propose and theoretically substantiate a method to study the nonlocal conductivity of two-dimensional electron systems (2DESs) using the tools of near-field microscopy. We show that the height-dependent polarizability of an illuminated near-field probe is substantially different for various transport regimes of charge carriers in a 2DES. For the hydrodynamic transport regime, the polarizability scales as z_0^{-2} , where z_0 is the elevation of the probe above the 2DES. Both for Drude and for classical ballistic regimes of conduction, the polarizability scales as z_0^{-3} . In the former case, the polarization is carrier density independent, while in the latter it largely depends on carrier density. More generally, we find that the polarizability of the probe is proportional to the Laplace transform of the wave-vector-dependent conductivity and the inverse dielectric function of the 2DES over the wave vectors q . Our results should provide a simple tool for studies of nonlocal conductivity in solids, which is challenging to address with other techniques.

DOI: [10.1103/PhysRevB.107.205409](https://doi.org/10.1103/PhysRevB.107.205409)

I. INTRODUCTION

The relations between the electric field and the current in solids are generally nonlocal, which implies that the current density at a given point $\mathbf{j}(\mathbf{r})$ can be affected by the field at remote positions $\mathbf{E}(\mathbf{r}')$:

$$\mathbf{j}(\mathbf{r}) = \int \sigma(\mathbf{r}, \mathbf{r}') \mathbf{E}(\mathbf{r}') d\mathbf{r}'. \quad (1)$$

The nonlocality comes from thermal or quantum motion of charge carriers. Formally, this motion results in explicit dependence of the conductivity kernel $\sigma(\mathbf{r}, \mathbf{r}')$ on positions \mathbf{r} and \mathbf{r}' . At zero frequency, the conductivity kernel is large only at distances $|\mathbf{r}' - \mathbf{r}|$ less than the electron mean free path. At finite frequencies, the kernel typically decays at the electron path during the field cycle $l_\omega = v_0/\omega$, where v_0 is the thermal or Fermi velocity of charge carriers [1]. At even smaller (quantum) distances $|\mathbf{r}' - \mathbf{r}|$, the conductivity kernel may possess extra features associated with Friedel oscillations [2,3] or cyclotron motion [4,5] of electrons in a magnetic field.

Once the nonlocal conductivity kernel $\sigma(\mathbf{r}, \mathbf{r}')$ is known, it may be tempting to decode the information about carrier dynamics from it [6]. Such a method may become a simple complement to complex angle-resolved photoelectron spectroscopy. Most straightforward ways to measure the nonlocal dielectric function rely on electron energy loss spectroscopy [7], which requires ultrahigh vacuum and atomically clean surfaces. There exist all-electrical methods for studies of nonlocal conduction, where current is injected between two contacts, while the voltage is measured between another two contacts [8–11]. Such a technique, however, is limited by the initially defined geometry of the contacts, and the nonlocal resistance signal may not have a simple and direct interpretation [12]. Recently, indirect evidence of transport nonlocality was theoretically revealed in height-dependent magnetic noise above two-dimensional (2D) electronic systems [13] and

magnets [14]. Measurements of local shot noise using near-field probes recently evidenced the nonlocal character of energy dissipation [15]; yet this quantitative observation was insufficient to distinguish the regime of carrier transport.

In recent years, great attention has been attracted to the technique of near-field optical microscopy by scattering from the tip [16]. It enables the reconstruction of optical properties in nonuniform structures [dielectric function $\varepsilon(\mathbf{r})$ or surface conductivity $\sigma(\mathbf{r})$] with resolution reaching $\sim 10^{-3}\lambda_0$ [17–20]. All such studies, however, assume the local relations between the current and the electric field, $\mathbf{j}(\mathbf{r}) \approx \sigma(\mathbf{r})\mathbf{E}(\mathbf{r})$. Attempts to extract the nonlocal conductivity (even in uniform structures) from near-field measurements are yet in their initial stage. In particular, the nonlocality of conductivity can affect the speed of collective excitations, namely, plasmons [21,22], which, in turn, can be extracted from polariton interferometry [23,24]. Such a technique allows one to extract the information about nonlocality only at “interlocked” values of frequency ω and wave vector q satisfying the plasmon dispersion relation.

In this paper, we substantiate theoretically a method for studies of nonlocal carrier dynamics from the near-field optical signals. We show that electromagnetic scattering from a near-field probe located at a small distance z_0 above a 2D conductor is strongly affected by the nonlocality of the conductivity kernel. For more precise formulation, we introduce the effective polarizability of the tip α_{eff} , which is the proportionality coefficient between dipole moment \mathbf{d} and incident field at the probe position $\mathbf{E}^{(i)}(z_0)$, $\mathbf{d}(z_0) = \alpha_{\text{eff}}(z_0)\mathbf{E}^{(i)}(z_0)$. We find that $\alpha_{\text{eff}}(z_0) - \alpha_{\text{eff}}(\infty)$ is a power-law function $\propto z_0^{-n}$. The exponent of this dependence n is linked to the asymptotics of Fourier-transformed nonlocal conductivity $\sigma_{2D}(\mathbf{q})$ at large field momenta \mathbf{q} . As a prototypical example, we consider the scaling of near-field signals for 2D electrons obeying the laws of drift and diffusion (Drude conduction), the classical ballistic motion, or the laws of hydrodynamics. We find that

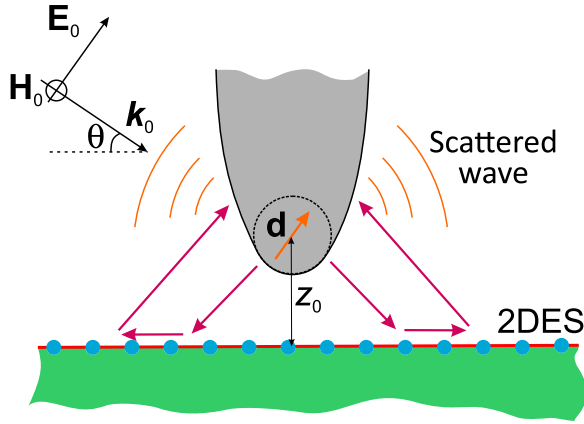


FIG. 1. Schematic of the setup. A near-field probe (gray) is illuminated by an incident plane wave. Its near field (magenta) is reflected by a two-dimensional electron system (2DES), which reacts to the field nonlocally. The reflected wave modifies the dipole moment of the probe \mathbf{d} . This dipole produces a scattered far field which carries information about the surface conductivity of the 2DES.

$\alpha_{\text{eff}} \propto z_0^{-3}$ in the two former cases and $\alpha_{\text{eff}} \propto z_0^{-2}$ in the case of hydrodynamics. More generally, we find that the induced dipole moment $d_z(z_0)$ of the near-field probe can be presented as a Laplace transform of nonlocal conductivity $\sigma_{2D}(q)$ divided by 2D dielectric function $\varepsilon_{2D}(q)$ with respect to the field momentum q .

II. SOLUTION OF THE SCATTERING PROBLEM FOR NONLOCAL CONDUCTIVITY

The studied system represents an extended two-dimensional electron system (2DES) located at $z = 0$ and a near-field probe elevated at height z_0 above it (Fig. 1). The in-plane coordinate of the probe is set as $\rho = 0$. The probe is illuminated by a plane wave with electric field $\mathbf{E}_0 e^{i\mathbf{k}_0 \cdot \mathbf{r} - i\omega t}$. It polarizes the probe and generates electromagnetic near fields with large spatial Fourier harmonics \mathbf{E}_q . These near fields are reflected from the 2DES; their reflection coefficient is generally determined by nonlocal conductivity $\sigma(\mathbf{q})$. Reflected waves modify the dipole moment of the probe \mathbf{d} and therefore modify its far-field radiation. One may suggest that the characteristic wave vector of tip-induced near fields is $q \lesssim z_0^{-1}$. By placing the tip at progressively smaller distances, one collects information about the surface conductivity at larger and larger wave vectors.

To justify the suggested scheme, we present an exact solution for the scattering problem presented in Fig. 1 with full account taken for conduction nonlocality. For analytical traceability, the tip is modeled as a point dipole with moment $\mathbf{d} = \{0, 0, d_z\}$. In the first stage, we find the fields in all space $\mathbf{E}(\mathbf{r})$ provided that \mathbf{d} is fixed and assuming no external illumination. A similar problem of dipole radiation above the nonlocal surface is known for bulk metals [25] but has not been reported for 2D. This is done, most conveniently, by solving the wave equation for the vector potential in the

Lorenz gauge:

$$\left(k_z^2 - \frac{\partial^2}{\partial z^2}\right) \mathbf{A}(\mathbf{q}, z) = \frac{4\pi}{c} [\mathbf{j}_{\text{dip}}(\mathbf{q})\delta(z - z_0) + \mathbf{j}_{2D}(\mathbf{q})\delta(z)]. \quad (2)$$

In the above equation, we have introduced the Fourier transform with respect to the in-plane coordinate, $\mathbf{A}(\mathbf{q}, z) = \int \mathbf{A}(\boldsymbol{\rho}, z) e^{i\mathbf{q}\cdot\boldsymbol{\rho}} d\boldsymbol{\rho}$, $k_z^2 = q^2 - k_0^2$ is the squared transverse wave vector, $k_0 = \omega/c$ is the wave number of the incident light, $\mathbf{j}_{\text{dip}}(\mathbf{q}) = -i\omega\mathbf{d}$ is the current density at the oscillating dipole, and $\mathbf{j}_{2D}(\mathbf{q})$ is the surface current density at the 2DES. We link it to the in-plane electric field via the nonlocal Ohm's law,

$$\mathbf{j}_{2D}(\mathbf{q}) = \sigma_{2D}(\mathbf{q})\mathbf{E}_{\parallel}(\mathbf{q}, z = 0), \quad (3)$$

while the electric field is obtained via the vector potential as

$$\mathbf{E}_{\parallel}(\mathbf{q}, z) = \frac{i}{k_0} [i\mathbf{q}(\nabla \cdot \mathbf{A}) + k_0^2 \mathbf{A}_{\parallel}]. \quad (4)$$

Combining the above equations, we arrive at a simple second-order equation for the vector potential with two delta sources on the right-hand side. The above equation is readily solved (Appendix A) with the following result:

$$A_z(\mathbf{q}, z) = A_{\text{dip}} e^{ik_z|z - z_0|}, \quad (5)$$

$$\mathbf{A}_{\parallel}(\mathbf{q}, z) = -A_{\text{dip}} e^{ik_z(|z| + z_0)} \frac{\mathbf{q}}{k_0} \frac{\eta(q)}{1 + \eta(q)k_z/k_0}. \quad (6)$$

Above, we have introduced the characteristic vector potential created by dipole source A_{dip} and dimensionless 2D conductivity $\eta(q)$:

$$A_{\text{dip}} = 2\pi \frac{k_0}{k_z} d, \quad (7)$$

$$\eta(q) = \frac{2\pi\sigma_{2D}(q)}{c}. \quad (8)$$

Several important properties of the fields created by a fixed dipole [(5) and (6)] should be mentioned before proceeding to an actual scattering problem. First of all, the net field cannot be presented as a superposition of the dipole field and its image field unless the 2DES is perfectly reflecting ($|\eta| \gg 1$). This holds even in the case of local 2D conductivity due to the explicit q dependence of the effective 2D dielectric function $\varepsilon_{2D}(q) = 1 + \eta(q)\sqrt{k_0^2 - q^2}/k_0$. Second, the field (6) carries information about the nonlocality of the 2D conductivity via the factors $\eta(q)$. However, most such information is lost when observing the radiated far field (see Appendix B for more details). Indeed, the radiative Fourier harmonics are bounded by $q < k_0$, while an appreciable spatial dispersion of conductivity emerges at $q \gtrsim \omega/v_0 \gg k_0$, where v_0 is the carrier Fermi velocity. Therefore, to access the full spatial dispersion, it is not sufficient to consider the radiation of a fixed dipole. It is rather necessary to go further and study the modifications of dipole polarizability in external fields.

In the second stage, we use the superposition principle to find the total field $\mathbf{E}^{(2)}$ created by external illumination, $\mathbf{E}^{(1)}$, and dipole with moment d_z , \mathbf{E} . We limit ourselves to the p -polarized incident fields and consider the near-field probe to be polarizable only in the vertical z direction. The only component of the electric field of interest is its z component,

and the superposition principle reads as

$$E_z^{(\Sigma)}(\mathbf{r}) = E_z^{(i)}(\mathbf{r}) + E_z(\mathbf{r}), \quad (9)$$

where the external illumination is due to incident and reflected waves, $E_z^{(i)}(\mathbf{r}) = E_0 \sin \theta (e^{-ik_0 \cos \theta z} + r_p e^{ik_0 \cos \theta z})$, θ is the gliding angle, and $r_p = [1 + 1/(\eta \cos \theta)]^{-1}$ is the reflection coefficient for the p -polarized wave.

In the last stage, we release the assumption of the fixed dipole moment and link it to the local field E_z at $\mathbf{r} = \mathbf{r}_0$ ($\rho = 0$, $z = z_0$) via the polarizability α :

$$\begin{aligned} d_z &= \alpha E_z(\mathbf{r}_0) \\ &= \alpha \left[E_z^{(i)}(z_0) + \int \frac{d^2 \mathbf{q}}{(2\pi)^2} \tilde{E}_z(\mathbf{q}, z_0) \right]. \end{aligned} \quad (10)$$

Certain care should be taken upon evaluation of the last integral. Strictly speaking, it diverges because the field created by the point dipole at its own origin is infinite. This self-action term should be subtracted (see Appendix C). As a result, the dipole is polarized according to the magnitude of smooth fields modified by the presence of the 2DES, denoted as $\tilde{E}_z(\mathbf{q}, z_0)$. Solving Eq. (10), which is linear with respect to \mathbf{d} , we find

$$d_z = \frac{\alpha}{1 - \alpha I_z} E_z^{(i)}(z_0), \quad (11)$$

where I_z is the polarization factor containing the information about nonlocal 2D conductivity:

$$I_z = \frac{1}{k_0} \int_0^\infty \frac{\eta(q)}{1 + \eta(q)k_z/k_0} q^3 e^{-2k_z z_0} dq. \quad (12)$$

The result coincides with that reported in Ref. [26] if expressed through wave-vector-dependent reflection coefficients.

An important property of the polarization factor I_z can be observed without specification of the transport model in the 2DES. The scaled 2D conductivity $\eta(q)$ in Eq. (12) appears both in the numerator and in the denominator. This implies that for large η , the polarizability of the probe approaches the universal limit, as it should for a perfectly reflecting surface. In most practical situations, this behavior is not realized, either because $\eta \ll 1$ at most typical electron densities or because $\eta(q)$ decays at large q . The only exception to this rule is expected for very high mobility 2DESs in GaAs quantum wells, where $\eta \sim 1$ can be reached [27].

Generally, the polarizability of the near-field probes is very small, of the order of r_{tip}^3 , where $r_{\text{tip}}^3 \sim 10$ nm is the curvature radius of the tip. This justifies the expansion of Eq. (11) in powers of α :

$$d_z = E_z^{(i)}(z_0) (\alpha + \alpha^2 I_z + \alpha^3 I_z^2 + \dots). \quad (13)$$

The linear-in- α term contains no information about near fields; it is sensitive only to the reflection of the incident plane wave from the uniform 2DES, r_p . The α^2 term is the largest one that carries information about the near-field reflection. It will be the focus of subsequent analysis, while the quantity αI_z will be called the effective polarizability. Practically, the

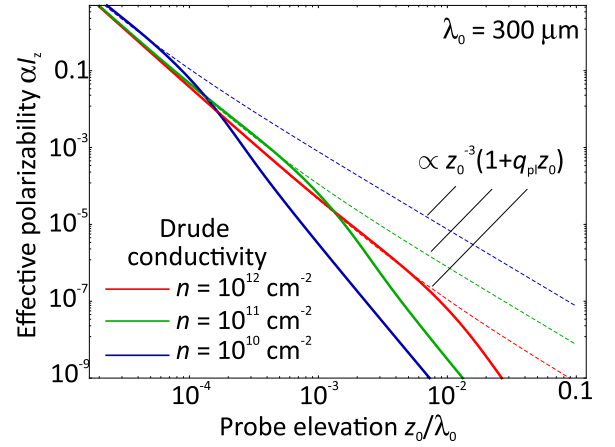


FIG. 2. Effective polarizability of the near-field probe αI_z vs the probe elevation z_0 (in units of free-space wavelength λ_0) for Drude conduction in a 2DES. Solid lines are the results of exact integration [Eq. (12)], and dashed lines are power-law asymptotes. Incident wave frequency $\omega/2\pi = 1$ THz, momentum relaxation time $\tau_p = 2$ ps, effective mass $m = 0.067m_0$, background dielectric constant $\epsilon_b = 4$, and tip radius $r_{\text{tip}} = 10$ nm.

linear-in- α contribution to the scattered far field is filtered out by modulating the elevation of the probe above the 2DES [16].

III. ANALYSIS OF THE INDUCED DIPOLE MOMENT FOR PARTICULAR TRANSPORT REGIMES

The dipole moment of the near-field probe contains information about nonlocal conductivity. Indeed, according to Eq. (12), I_z is a convolution of the wave-vector-dependent conductivity $\sigma(q)$, the inverse 2D permittivity, and the height-dependent factor $e^{-2\sqrt{q^2 - k_0^2} z_0}$. We shall further analyze the height dependence of effective polarizability and show that it indeed depends on the regime of carrier transport in the 2DES.

Before proceeding, we note that in the far-field zone, $z_0 \gg \lambda_0$, the effective polarizability displays an inverse proportionality to z_0 . This result is independent of the particular transport regime in the 2DES. Indeed, in the far zone, the wave vectors $q \leq k_0$ yield the dominant contribution to the integral (12). The spatial dispersion of conductivity does not develop at such small wave vectors. For this reason, all further considerations will be restricted to the near-field region $k_0 z_0 \ll 1$.

A. Drude conductivity

The simplest model of 2DES conductivity is the Drude model, wherein the spatial dispersion is completely absent:

$$\sigma_D = \frac{ne^2}{m_e(\omega + i/\tau_p)}, \quad (14)$$

where n is the density of 2D electrons, m_e is their effective mass, and τ_p is the momentum relaxation time. The resulting height-dependent effective polarizability is shown in Fig. 2 for three characteristic carrier densities, $n = 10^{12}$, 10^{11} , and 10^{10} cm^{-2} , and $r_{\text{tip}} = 10$ nm. The overall dependence has two distinct regions with different height scalings.

The effective polarizability in this case is evaluated analytically to yield

$$I_z = \frac{i\pi\sigma_D}{c} \frac{q_{\text{pl}}}{k_0} \left\{ q_{\text{pl}}^3 e^{-2q_{\text{pl}}z_0} (\text{Ei}(2q_{\text{pl}}z_0) - i\pi) - \frac{q_{\text{pl}}z_0(2q_{\text{pl}}z_0 + 1) + 1}{4z_0^3} \right\}, \quad (15)$$

where it was convenient to introduce the wave vector of 2D plasmons:

$$q_{\text{pl}} = \frac{\epsilon_b\omega(\omega + i/\tau_p)}{2\pi n_e e^2/m_e}. \quad (16)$$

The only dimensionless parameter governing the principal height dependence of I_z is the ratio of the probe elevation and the 2D plasmon wavelength. At moderate heights, $q_{\text{pl}}z_0 \gg 1$ (but still $z_0k_0 \ll 1$), the height dependence follows the z_0^{-4} asymptotics:

$$I_z(q_{\text{pl}}z_0 \gg 1) \approx \frac{3i\pi}{8} \frac{\sigma_D}{c} \frac{1}{k_0 z_0^4}. \quad (17)$$

At even smaller distances, $q_{\text{pl}}z_0 \ll 1$, the scaling of the polarizability is inverse cubic:

$$I_z(q_{\text{pl}}z_0 \ll 1) \approx \frac{\epsilon_b}{8z_0^3} (1 + q_{\text{pl}}z_0). \quad (18)$$

It is remarkable that the leading term of the induced dipole moment is independent of the carrier density at small heights. Indeed, at large q , the dielectric function of the 2DES, ϵ_{2D} , is directly proportional to the conductivity. The integrand in (12) becomes independent of the surface conductivity; we may speculate that the 2D conductor acts as a perfect mirror in this limit.

B. Hydrodynamic transport

The hydrodynamic transport mode in a 2DES is established if the carrier-carrier collisions are so rapid that electrons behave as a viscous fluid. Parametrically, this corresponds to $\omega\tau_{ee} \ll 1$ and $ql_{\text{fp}} \ll 1$, where τ_{ee} is the mean free time between electron-electron collisions and $l_{\text{fp}} = v_0\tau_{ee}$ is the mean free path [28,29]. In this limit, the conductivity is given by

$$\sigma_{\text{hd}} = \frac{ne^2\omega/m_e}{\omega(\omega + i/\tau_p) - v_0^2q^2/2}. \quad (19)$$

The full plot of polarization factor I_z in such a transport mode is shown in Fig. 3. At very low heights, $z_0 \lesssim v_0/\omega$, the scaling is inverse quadratic (compared with inverse cubic for Drude conductivity). The reason for this difference lies in the asymptotic behavior of the conductivity $\sigma_{\text{hd}} \propto q^{-2}$ at large wave vectors. The conductivity decays very rapidly at large wave vectors (small heights); thus the 2DES does not actively reflect the electromagnetic near fields. As a result, it fails to build up a large dipole moment of the probe. This contrasts to the Drude case, when I_z diverged as z_0^{-3} at very small heights.

Taking only the leading terms in the expansion of σ_{hd} at large q , we get the following asymptotic behavior:

$$I(z_0) \approx \frac{i\pi}{2} \frac{\sigma_\omega}{c} \frac{k_s^2}{k_0 z_0^2}, \quad (20)$$

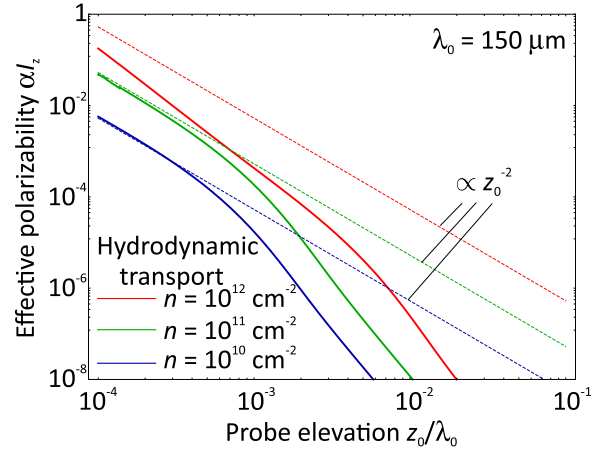


FIG. 3. Effective polarizability of the near-field probe αI_z vs the probe elevation z_0 for hydrodynamic transport in a 2DES. Solid lines are the results of exact integration [Eq. (12)], and dashed lines are power-law asymptotes. Incident wave frequency $\omega/2\pi = 2$ THz, momentum relaxation time $\tau_p = 2$ ps, effective mass $m = 0.067m_0$, background dielectric constant $\epsilon_b = 4$, tip radius $r_{\text{tip}} = 10$ nm, and Fermi velocity $v_0 = 10^6$ m/s.

where $\sigma_\omega = ne^2/m_e\omega$ and we have introduced the wave vector of sound waves supported by the 2DES, $k_s = \sqrt{2}\omega/v_0$. This asymptotic behavior, shown in Fig. 3 with dashed lines, matches well the full expression for I_z at small heights.

C. Ballistic transport

Another limiting case for spatially dispersive conductivity of a 2DES is realized for very long free paths, both for carrier collisions with disorder and with each other, $\omega\tau_p \gg 1$ and $\omega\tau_{ee} \gg 1$. If the frequencies and wave vectors still lie in the classical domain, $\omega \ll \epsilon_F/v_0$ and $q \ll k_F$, the ballistic conductivity can be found from the kinetic equation with the following result [30]:

$$\sigma_{\text{bal}} = \frac{ne^2/m_e}{\sqrt{(\omega + i/\tau_p)^2 - v_0^2q^2}}. \quad (21)$$

For short wavelengths, $q > \omega/v_0$, the conductivity is purely real even at ultimately scarce collisions. This is a manifestation of the Landau damping effect. In the short-wavelength limit, the decay of ballistic conductivity ($\sigma_{\text{bal}} \propto q^{-1}$) is intermediate between those in hydrodynamic ($\sigma_{\text{hd}} \propto q^{-2}$) and Drude ($\sigma_D \propto q^0$) regimes. Taking such a limit for the conductivity, we evaluate the asymptotics of I_z at very small height:

$$I_z \approx \frac{\epsilon_b}{4z_0^3} \frac{p}{1 + ip}, \quad p = \epsilon_b^{-1} \frac{2\pi\sigma_\omega}{v_0}. \quad (22)$$

At a first glance, the scaling of induced dipole moment $I_z \propto z_0^{-3}$ for ballistic transport (Fig. 4) is not different from that for Drude conductivity. However, ballistic conduction leads to a carrier-density-dependent prefactor in the induced dipole moment, while for Drude conduction the asymptotics is density independent. Experimentally, these two transport modes can be conveniently distinguished by varying the 2D electron density with the gate voltage.

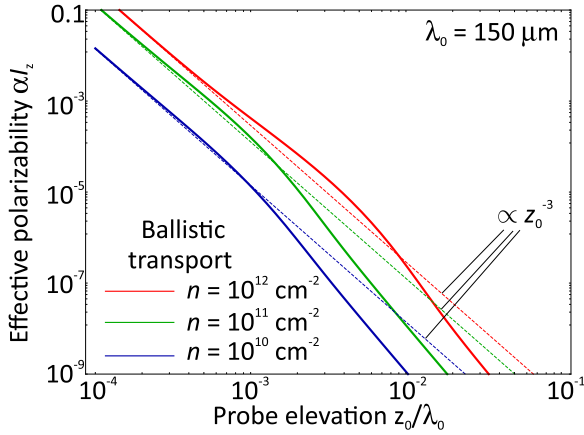


FIG. 4. Effective polarizability of the near-field probe αI_z vs the probe elevation z_0 for ballistic transport in a 2DES. Solid lines are the results of exact integration [Eq. (12)], and dashed lines are power-law asymptotes. Incident wave frequency $\omega/2\pi = 2$ THz, momentum relaxation time $\tau_p = 2$ ps, effective mass $m = 0.067m_0$, background dielectric constant $\epsilon_b = 4$, tip radius $r_{\text{tip}} = 10$ nm, and Fermi velocity $v_0 = 10^6$ m/s.

IV. DISCUSSION AND POSSIBLE GENERALIZATIONS

The possible generalizations of our work can be categorized as “kinetic” ones and “electrodynamic” ones. In the first case, one takes a more detailed view of the microscopic origin of the nonlocal conductivity in different transport regimes. In the second case, one can apply more sophisticated models of light scattering by the tip and the surface.

From the kinetic viewpoint, the obtained results are valid both for graphene and a 2DES with parabolic bands, such as quantum wells based on III-V compounds. In the former case, the carrier effective mass in expressions for the conductivity [(14), (19), and (21)] should be interpreted as ϵ_F/v_0^2 , where ϵ_F is the carrier Fermi energy and $v_0 = 10^6$ m/s is the constant Fermi velocity. In the case of a parabolic-band 2DES, the Fermi velocity is dependent on the Fermi energy: $v_0 = \sqrt{2m_e\epsilon_F}$, where m_e is the constant effective mass.

It is possible to extend the discussion to the quantum regimes of electron conductivity realized at $q \sim k_F$, where k_F is the Fermi wave vector. While the detailed analysis of such cases is beyond the scope of this paper, we note a very different scaling of ultraquantum conductivities for graphene and a parabolic-band 2DES. In the case of graphene, $\sigma(q \gg k_F) \propto q^{-1}$ [22], while in the case of a parabolic-band 2DES, $\sigma(q \gg k_F) \propto q^{-5}$ [30]. A rapid drop in the conductivity at large q in a parabolic-band 2DES should lead to height-independent behavior of I_z at $z_0 k_F \sim 1$.

Strictly speaking, the method presented works fine only for translation-invariant 2DESs, i.e., those without roughness and defects. Only in such cases is the concept of wave-vector-dependent conductivity well defined. At the same time, we expect that the method would work both for very long scale roughness and for very short scale roughness. In the former case, when the roughness correlation length l_c exceeds the free path $v_0\tau_p$ and v_0/ω , the nonlocal conductivity can be measured in each uniform section of the 2DES. In the latter case, when the roughness correlation length l_c is the shortest

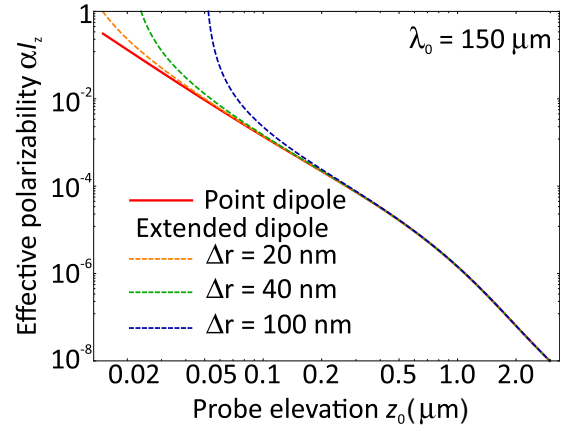


FIG. 5. Effect of finite probe size on the scaling of effective polarizability αI_z . The solid line corresponds to the point dipole model, and dashed lines correspond to the elongated dipole model with various sizes of the dipole Δr . All calculations correspond to the Drude conductivity with $n = 10^{12}$ cm^{-2} , $\omega/2\pi = 2$ THz, $\tau_p = 2$ ps, and $\alpha = 10^{-24}$ cm^{-3} .

length scale in the problem, the method would measure the disorder-averaged nonlocal conductivity, where the effects of roughness are absorbed in scattering time τ_p .

From the electrodynamic viewpoint, the presented calculation was performed for a point-dipole model of a near-field tip. We realize that interpretation of the current experimental results requires more complex models, such as an elongated dipole [31], exact conformal mappings [32], or fully numerical simulations [26]. Without going into the details of such models, we can account for “elongation” of the dipole at the probe tip by modeling it as two charges, Q and $-Q$, separated by a finite distance Δr . The dipole moment can be still estimated as $Q\Delta r = \alpha E(z_0)$, where α is the tip polarizability and $E(z_0)$ is the electric field between the two charges. The expression for the dipole moment in such a situation is slightly modified:

$$I_z = \frac{1}{k_0} \int_0^\infty \frac{2\pi i \sigma(q, \omega)}{c} \frac{\sinh q\Delta r}{q\Delta r} e^{-2qz_0} \frac{q^3 dq}{\epsilon_{2D}(q, \omega)}. \quad (23)$$

The resulting dependence of polarizability I_z on height z_0 at various dipole elongations Δr is shown in Fig. 5. Naturally, the range of accessible heights for such a model is limited to $z_0 > \Delta r/2$. Otherwise, the lower charge falls below the 2DES plane, and the expression (23) formally diverges. It is also instructive that for small heights and relatively large elongation ($|z_0 - \Delta r/2| \ll z_0$) we restore the monopole model of the probe. In this case, only the lower charge interacts efficiently with the 2DES, and scaling of I_z with height can be different.

The previous calculations have been performed for identical dielectric permittivities of media above and below the 2DES, while typical 2D materials reside on substrates. This fact can also be accounted for in future calculations. We can expect in advance that substrates with a very large dielectric constant would screen out the effect of 2D conductivity (no matter whether it is local or not) on probe polarizability.

So far, we have considered the behavior of effective probe polarizability for selected modes of transport. It is now tempting to restore the full spatial dispersion of conductiv-

ity $\sigma(q, \omega)$ from the measured complex quantity $I_z(z_0)$. This problem is equivalent to the solution of the integral equation

$$I_z(z_0) = \frac{1}{k_0} \int_0^\infty f(q) q^3 e^{-2qz_0} dq \quad (24)$$

with respect to the dimensionless function

$$f(q) = \frac{2\pi i \sigma(q, \omega)/c}{\epsilon_{2D}(q, \omega)}. \quad (25)$$

In essence, the problem lies in finding the numerical inverse Laplace transform [33]. Strictly speaking, this inversion requires knowledge of $I_z(z_0)$ at complex values z_0 which are not accessible experimentally. Nevertheless, an experimentally measured dependence $I_z(z_0)$ can be approximately *fitted* as a power series in z_0 with negative powers:

$$I_z(z_0) = \sum_{n=0}^{N_{\max}} a_n z_0^{-n-1}. \quad (26)$$

Above, the coefficients a_n have to be determined by the numerical fitting procedure, and N_{\max} is chosen to ensure fitting to the desired accuracy. Now, the solution of integral equation (24) can be sought for as a series in powers of q :

$$f(q) = \sum_{n=0}^{N_{\max}} c_n q^{n-3}. \quad (27)$$

Substituting the ansatz (27) into the right-hand side of the integral equation (24), using the fitted series (26) for the left-hand side, and equating the coefficients at equal powers of z_0 , we get

$$c_n = \frac{a_n k_0}{2^{n+1} n!}. \quad (28)$$

Expression (28) establishes the relation between the power series of the nonlocal conductivity in terms of q and the power series of the probe polarizability in terms of height z_0 .

V. CONCLUSIONS

We have demonstrated the possibility to distinguish between transport regimes in two-dimensional electron systems via the height dependence of the near-field tip dipole moment. The height dependence follows the z_0^{-3} law for classical ballistic and Drude regimes of conduction in 2DESs. In the former case, the prefactor of the power law is dependent on the carrier density, and in the latter case it is density independent. For the hydrodynamic regime of carrier transport, the buildup of dipole moment at small heights is not as rapid and obeys the z_0^{-3} law.

ACKNOWLEDGMENTS

The research was supported by the Grant No. 21-72-10163 of the Russian Science Foundation. The authors thank Alexey Y. Nikitin and Andrei Bylinkin for helpful discussions and Zhanna Devizorova for assistance with calculations.

APPENDIX A: SOLUTION OF THE WAVE EQUATION FOR A FIXED DIPOLE SOURCE

Here, we solve the wave equation for the vector potential $\mathbf{A}(\mathbf{q}, z)$ if the dipole moment d_z of the probe is known and fixed. Expressing the currents due to the dipole and the 2DES in Eq. (2) explicitly, we find

$$\left(k_z^2 - \frac{\partial^2}{\partial z^2}\right) \mathbf{A}(\mathbf{q}, z) = \frac{4\pi}{c} [-i\omega \mathbf{d} \delta(z - z_0) + \mathbf{j}_{2D}(\mathbf{q}) \delta(z)], \quad (A1)$$

where we have introduced the z component of the wave vector $k_z^2 = k_0^2 - q^2$.

The equation for the component of the vector potential A_z is decoupled from currents in the 2DES, as the latter have no out-of-plane component. It has a simple form:

$$k_z^2 A_z + \frac{\partial^2 A_z}{\partial z^2} = \frac{4\pi i \omega}{c} d_z \delta(z - z_0), \quad (A2)$$

where we have skipped the arguments (\mathbf{q}, z) . The solution of (5) decaying at $z \rightarrow \pm\infty$ is given by

$$A_z = A_{\text{dip}} e^{i k_z |z - z_0|}, \quad (A3)$$

$$A_{\text{dip}} = 2\pi \frac{k_0}{k_z} d_z. \quad (A4)$$

We now proceed to the in-plane component of the vector potential, which is governed by the currents in the 2DES solely:

$$k_z^2 \mathbf{A}_{\parallel} + \frac{\partial^2 \mathbf{A}_{\parallel}}{\partial z^2} = -\frac{4\pi}{c} \mathbf{j}_{2D} \delta(z). \quad (A5)$$

A formal solution of this equation has a simple exponential form:

$$\mathbf{A}_{\parallel}(\mathbf{q}, z) = \mathbf{A}_{\parallel}(\mathbf{q}, 0) e^{i k_z |z|}, \quad (A6)$$

$$\mathbf{A}_{\parallel}(\mathbf{q}, 0) = \frac{2\pi i}{c k_z} \mathbf{j}_{2D}(\mathbf{q}). \quad (A7)$$

In order to express the in-plane vector potential via the dipole moment, we use the nonlocal Ohm's law for the 2D current density (3) along with the expression for the \mathbf{E} field via the vector potential in the Lorenz gauge (4). In extended form, it reads as

$$\mathbf{E}_{\parallel} = i k_0 \mathbf{A}_{\parallel} - \frac{\mathbf{q}}{k_0} \left(i q \mathbf{A}_{\parallel} + \frac{\partial A_z}{\partial z} \right). \quad (A8)$$

The self-consistency procedure mentioned above leads us to the explicit expression for \mathbf{A}_{\parallel} :

$$\mathbf{A}_{\parallel}(\mathbf{q}, z) = -A_{\text{dip}} e^{i k_z (|z| + z_0)} \frac{\mathbf{q}}{k_0} \frac{\eta(q)}{1 + \eta(q) k_z / k_0}. \quad (A9)$$

APPENDIX B: RADIATION OF A DIPOLE ABOVE A 2DES

To find the power radiated by a dipole above a 2DES, it is necessary to compute the flux of the Poynting vector through the surface enclosing the dipole. Due to the cylindrical symmetry of the problem, it is convenient to enclose the dipole

and 2DES in a cylinder with the axis along the z direction and radius $R \rightarrow \infty$. The height of the cylinder H is chosen such that $\lambda_0 + z_0 \ll H \ll R$. Under such conditions, the energy flux through the side surfaces of the cylinder can be neglected. The power flowing through the top surface of the cylinder can be expressed as

$$P_{\uparrow} = \int 2\pi \rho d\rho S_z(\rho) \equiv \frac{c}{2\pi} \int 2\pi \rho d\rho \operatorname{Re} [E_{\rho} H_{\varphi}^*], \quad (\text{B1})$$

where the components of the electric and magnetic vector are now expressed in the cylindrical coordinates.

To compute the power flow, we first switch to full coordinate representation of the vector potential. Once $A_z(\mathbf{q}, z)$ and $\mathbf{A}_{\parallel}(\mathbf{q}, z)$ are known [Eqs. (5) and (6)], the ρ -dependent fields are found using inverse Fourier transforms:

$$\begin{aligned} A_z(\rho, z) &= \frac{1}{(2\pi)^2} \int A_z(\mathbf{q}, z) e^{i\mathbf{q}\rho} d\mathbf{q} \\ &= \int \frac{2\pi q dq}{(2\pi)^2} J_0(q\rho) A_z(q, z), \end{aligned} \quad (\text{B2})$$

$$\begin{aligned} \mathbf{A}_{\parallel}(\rho, z) &= \frac{1}{(2\pi)^2} \int \mathbf{A}_{\parallel}(\mathbf{q}, z) \mathbf{n}_{\mathbf{q}} e^{i\mathbf{q}\rho} d\mathbf{q} \\ &= \mathbf{n}_{\rho} \int \frac{2\pi q dq}{(2\pi)^2} iJ_1(q\rho) A_{\parallel}(\mathbf{q}, z). \end{aligned} \quad (\text{B3})$$

The necessary components of electric and magnetic fields, E_{ρ} and H_{φ} , are found from (B2) and (B3) using the definitions $\mathbf{H} = [\nabla \times \mathbf{A}]$ and $\mathbf{E} = ik_0 \mathbf{A} - \nabla \varphi$:

$$H_{\varphi}(\rho, z) = \frac{\partial A_{\rho}}{\partial z} - \frac{\partial A_z}{\partial \rho}, \quad (\text{B4})$$

$$E_{\rho}(\rho, z) = \frac{i}{k_0} \frac{\partial}{\partial z} \left(\frac{\partial A_z}{\partial \rho} - \frac{\partial A_{\rho}}{\partial z} \right). \quad (\text{B5})$$

We introduce the expressions for electric and magnetic fields (B2)–(B5) into the integral for the power flow (B1) and use the orthogonality relation:

$$\int_0^{\infty} \rho d\rho J_{\nu}(q\rho) J_{\nu}(q'\rho) = \frac{1}{q} \delta(q - q'). \quad (\text{B6})$$

This results in the following expression for the power flow:

$$P_{\uparrow} = \frac{c}{(2\pi)^2} \int_0^{k_0} q dq \frac{k_z}{k_0} |k_z A_{\parallel}(q, z) - q A_z(q, z)|^2. \quad (\text{B7})$$

The integration limits cover only a finite range of wave vectors $q \in [0, k_0]$. Waves with larger wave vectors are evanescent and do not contribute to the flow.

After expressing all fields via the source dipole moment d_z , the power flow acquires a very simple form:

$$\begin{aligned} P_{\uparrow} &= c |d_z|^2 \int_0^{k_0} q^3 dq \frac{k_0}{k_z} \left| 1 + \frac{e^{2ik_z z_0}}{1 + k_0/(\eta k_z)} \right|^2 \\ &= c |d_z|^2 k_0^4 \int_0^1 (1 - \tau^2) d\tau \left| 1 + \frac{e^{2i\tau(k_0 z_0)}}{1 + 1/(\eta \tau)} \right|^2. \end{aligned} \quad (\text{B8})$$

It is easy to verify that Eq. (B8) reproduces the known limiting cases. For a nearly transparent 2DES, $\eta \ll 1$, one gets $P = 2\omega^4 |d_z|^2 / 3c^3$, which is half of the full power of dipole emission (the other half is emitted through the bottom surface of the cylinder). For a mirror-type 2DES, $\eta \gg 1$, one obtains

$$P_{\uparrow, \text{mirror}} = \frac{2\omega^4 |d_z|^2}{c^3} \left(\frac{2}{3} + \frac{1}{(k_0 z_0)^2} - \frac{\sin 2k_0 z_0}{2(k_0 z_0)^3} \right), \quad (\text{B9})$$

which corresponds to the fourfold enhancement of radiated power due to in-phase oscillation of the original dipole and its image. For finite values of η , the radiated power is readily evaluated numerically.

Strictly speaking, the scaled 2D conductivity in Eq. (B8) depends on wave vector $\eta \equiv \eta(q)$. However, radiative components are limited to a very narrow range $q \in [0, k_0]$, such that spatial dispersion of the conductivity is not yet developed. As a result, η in Eq. (B8) can be treated as a constant $\eta(q = 0)$.

APPENDIX C: POLARIZABILITY OF A DIPOLE ABOVE A 2DES IN THE PRESENCE OF EXTERNAL ILLUMINATION

An illuminated dipole is polarized according to the total field, which is composed of the external illumination field $\mathbf{E}^{(i)}$ and the field created by the dipole itself in the presence of the 2DES, $\tilde{\mathbf{E}}$:

$$d_z = \alpha \left[E_z^{(i)}(z_0) + \int \frac{d^2 \mathbf{q}}{(2\pi)^2} \tilde{E}_z(\mathbf{q}, z_0) \right]. \quad (\text{C1})$$

The Fourier representation for the field $E_z(\mathbf{q}, z)$ can be obtained from the known vector potentials $A_z(\mathbf{q}, z)$ and $\mathbf{A}_{\parallel}(\mathbf{q}, z)$ [Eqs. (5) and (6)]:

$$E_z(\mathbf{q}, z) = \left(ik_0 + \frac{i}{k_0} \frac{\partial^2}{\partial z^2} \right) A_z(\mathbf{q}, z) - \frac{\partial}{\partial z} \frac{\mathbf{q} \mathbf{A}_{\parallel}(\mathbf{q}, z)}{k_0}. \quad (\text{C2})$$

The first and second terms of Eq. (C2) correspond to the part of the dipole field that is singular at $z \rightarrow z_0$. The third term is nonsingular. Physically, it corresponds to the evanescent field of the dipole after its reflection from the 2DES. This is further confirmed by the fact that \mathbf{A}_{\parallel} is proportional to 2D sheet conductivity $\eta(q)$ [see Eq. (6)]. Upon computation of the dipole moment, only the last term in the expression for the field (C2) should be taken into account:

$$\tilde{E}_z(\mathbf{q}, z) = -\frac{\partial}{\partial z} \frac{\mathbf{q} \mathbf{A}_{\parallel}(\mathbf{q}, z)}{k_0}. \quad (\text{C3})$$

Introducing \mathbf{A}_{\parallel} from Eq. (6) into (C3), we arrive at expression (12) for the effective polarizability.

[1] E. M. Lifshitz and L. P. Pitaevskii, *Physical Kinetics*, Course of Theoretical Physics Vol. 10 (Butterworth-Heinemann, Oxford, 1981).

[2] V. V. Cheianov and V. I. Fal'ko, Friedel Oscillations, Impurity Scattering, and Temperature Dependence of Resistivity in Graphene, *Phys. Rev. Lett.* **97**, 226801 (2006).

- [3] W. E. Liu, H. Liu, and D. Culcer, Screening, Friedel oscillations, and low-temperature conductivity in topological insulator thin films, *Phys. Rev. B* **89**, 195417 (2014).
- [4] K. W. Chiu and J. J. Quinn, Plasma oscillations of a two-dimensional electron gas in a strong magnetic field, *Phys. Rev. B* **9**, 4724 (1974).
- [5] D. A. Bandurin, E. Mönch, K. Kapralov, I. Y. Phinney, K. Lindner, S. Liu, J. H. Edgar, I. A. Dmitriev, P. Jarillo-Herrero, D. Svintsov, and S. D. Ganichev, Cyclotron resonance overtones and near-field magnetoabsorption via terahertz Bernstein modes in graphene, *Nat. Phys.* **18**, 462 (2022).
- [6] D. N. Basov, M. M. Fogler, A. Lanzara, F. Wang, and Y. Zhang, Colloquium: Graphene spectroscopy, *Rev. Mod. Phys.* **86**, 959 (2014).
- [7] A. Koitzsch, A.-S. Pawlik, C. Habenicht, T. Klaproth, R. Schuster, B. Büchner, and M. Knupfer, Nonlocal dielectric function and nested dark excitons in MoS₂, *npj 2D Mater. Appl.* **3**, 41 (2019).
- [8] A. Roth, C. Brüne, H. Buhmann, L. W. Molenkamp, J. Maciejko, X.-L. Qi, and S.-C. Zhang, Nonlocal transport in the quantum spin Hall state, *Science* **325**, 294 (2009).
- [9] G. M. Gusev, E. B. Olshanetsky, Z. D. Kvon, A. D. Levin, N. N. Mikhailov, and S. A. Dvoretzky, Nonlocal Transport Near Charge Neutrality Point in a Two-Dimensional Electron-Hole System, *Phys. Rev. Lett.* **108**, 226804 (2012).
- [10] D. A. Bandurin, A. V. Shytov, L. S. Levitov, R. K. Kumar, A. I. Berdyugin, M. Ben Shalom, I. V. Grigorieva, A. K. Geim, and G. Falkovich, Fluidity onset in graphene, *Nat. Commun.* **9**, 4533 (2018).
- [11] A. S. Mayorov, R. V. Gorbachev, S. V. Morozov, L. Britnell, R. Jalil, L. A. Ponomarenko, P. Blake, K. S. Novoselov, K. Watanabe, T. Taniguchi, and A. K. Geim, Micrometer-scale ballistic transport in encapsulated graphene at room temperature, *Nano Lett.* **11**, 2396 (2011).
- [12] K. G. Nazaryan and L. Levitov, Robustness of vorticity in electron fluids, *arXiv:2111.09878*.
- [13] K. Agarwal, R. Schmidt, B. Halperin, V. Oganessian, G. Zaránd, M. D. Lukin, and E. Demler, Magnetic noise spectroscopy as a probe of local electronic correlations in two-dimensional systems, *Phys. Rev. B* **95**, 155107 (2017).
- [14] H. Fang, S. Zhang, and Y. Tserkovnyak, Generalized model of magnon kinetics and subgap magnetic noise, *Phys. Rev. B* **105**, 184406 (2022).
- [15] Q. Weng, S. Komiyama, L. Yang, Z. An, P. Chen, S.-A. Biehs, Y. Kajihara, and W. Lu, Imaging of nonlocal hot-electron energy dissipation via shot noise, *Science* **360**, 775 (2018).
- [16] D. Richards, A. Zayats, F. Keilmann, and R. Hillenbrand, Near-field microscopy by elastic light scattering from a tip, *Philos. Trans. R. Soc. London Ser. A* **362**, 787 (2004).
- [17] H. G. Frey, S. Witt, K. Felderer, and R. Guckenberger, High-Resolution Imaging of Single Fluorescent Molecules with the Optical Near-Field of a Metal Tip, *Phys. Rev. Lett.* **93**, 200801 (2004).
- [18] A. J. Huber, F. Keilmann, J. Wittborn, J. Aizpurua, and R. Hillenbrand, Terahertz near-field nanoscopy of mobile carriers in single semiconductor nanodevices, *Nano Lett.* **8**, 3766 (2008).
- [19] A. A. Govyadinov, I. Amenabar, F. Huth, P. S. Carney, and R. Hillenbrand, Quantitative measurement of local infrared absorption and dielectric function with tip-enhanced near-field microscopy, *J. Phys. Chem. Lett.* **4**, 1526 (2013).
- [20] A. A. Govyadinov, S. Mastel, F. Golmar, A. Chuvilin, P. S. Carney, and R. Hillenbrand, Recovery of permittivity and depth from near-field data as a step toward infrared nanotomography, *ACS Nano* **8**, 6911 (2014).
- [21] V. Ryzhii, Terahertz plasma waves in gated graphene heterostructures, *Jpn. J. Appl. Phys.* **45**, 923 (2006).
- [22] E. H. Hwang and S. Das Sarma, Dielectric function, screening, and plasmons in two-dimensional graphene, *Phys. Rev. B* **75**, 205418 (2007).
- [23] M. B. Lundeberg, Y. Gao, R. Asgari, C. Tan, B. Van Duppen, M. Autore, P. Alonso-González, A. Woessner, K. Watanabe, T. Taniguchi, R. Hillenbrand, J. Hone, M. Polini, and F. H. L. Koppens, Tuning quantum nonlocal effects in graphene plasmonics, *Science* **357**, 187 (2017).
- [24] A. Charnukha, A. Sternbach, H. T. Stinson, R. Schlereth, C. Brüne, L. W. Molenkamp, and D. N. Basov, Ultrafast nonlocal collective dynamics of Kane plasmon-polaritons in a narrow-gap semiconductor, *Sci. Adv.* **5**, eaau9956 (2019).
- [25] R. Fuchs and R. G. Barrera, Dynamical response of a dipole near the surface of a nonlocal metal, *Phys. Rev. B* **24**, 2940 (1981).
- [26] A. S. McLeod, P. Kelly, M. D. Goldflam, Z. Gainsforth, A. J. Westphal, G. Dominguez, M. H. Thiemens, M. M. Fogler, and D. N. Basov, Model for quantitative tip-enhanced spectroscopy and the extraction of nanoscale-resolved optical constants, *Phys. Rev. B* **90**, 085136 (2014).
- [27] V. M. Muravev, P. A. Gusikhin, I. V. Andreev, and I. V. Kukushkin, Novel Relativistic Plasma Excitations in a Gated Two-Dimensional Electron System, *Phys. Rev. Lett.* **114**, 106805 (2015).
- [28] I. M. Khalatnikov and A. A. Abrikosov, The theory of a fermi liquid (the properties of liquid ³He at low temperatures), *Rep. Prog. Phys.* **22**, 329 (1959).
- [29] D. Svintsov, Hydrodynamic-to-ballistic crossover in Dirac materials, *Phys. Rev. B* **97**, 121405(R) (2018).
- [30] F. Stern, Polarizability of a Two-Dimensional Electron Gas, *Phys. Rev. Lett.* **18**, 546 (1967).
- [31] A. Cvitkovic, N. Ocelic, and R. Hillenbrand, Material-specific infrared recognition of single sub-10 nm particles by substrate-enhanced scattering-type near-field microscopy, *Nano Lett.* **7**, 3177 (2007).
- [32] S. T. Chui, X. Chen, M. Liu, Z. Lin, and J. Zi, Scattering of electromagnetic waves from a cone with conformal mapping: Application to scanning near-field optical microscope, *Phys. Rev. B* **97**, 081406(R) (2018).
- [33] B. Davies and B. Martin, Numerical inversion of the Laplace transform: a survey and comparison of methods, *J. Comput. Phys.* **33**, 1 (1979).